J. Fluid Mech. (1986), *vol.* 163, *pp.* 257–282
Printed in Great Britain

On the instability of a three-dimensional attachment-line boundary layer: weakly nonlinear theory and a numerical approach

By PHILIP HALL†
Mathematics Department, University of Exeter, North Park Road, Exeter, England

AND MUJEEB R. MALIK‡
High Technology Corporation, Hampton, VA 23666

(Received 8 January 1985)

The instability of a three-dimensional attachment-line boundary layer is considered in the nonlinear regime. Using weakly nonlinear theory, it is found that, apart from a small interval near the (linear) critical Reynolds number, finite-amplitude solutions bifurcate subcritically from the upper branch of the neutral curve. The time-dependent Navier–Stokes equations for the attachment-line flow have been solved using a Fourier–Chebyshev spectral method and the subcritical instability is found at wavenumbers that correspond to the upper branch. Both the theory and the numerical calculations show the existence of supercritical finite-amplitude (equilibrium) states near the lower branch which explains why the observed flow exhibits a preference for the lower branch modes. The effect of blowing and suction on nonlinear stability of the attachment-line boundary layer is also investigated.

1. Introduction

Our concern is with the weakly nonlinear and fully nonlinear stability of a three-dimensional attachment-line boundary layer obtained by introducing a crossflow into the classical Hiemenz stagnation-point boundary-layer solution. The resulting flow has a constant boundary-layer thickness and is in fact an exact solution of the Navier–Stokes equations. Thus, it is not necessary for us to obtain a self-consistent asymptotic solution of the instability problem based on a high-Reynolds-number approximation. In fact, the flow we consider is the first-order boundary-layer solution corresponding to the flow near the leading edge of a swept wing. If the flow over the wing is required to be laminar, then it is, of course, essential that the attachment-line flow be stable so that the problem we consider is of direct relevance to laminar flow control.

The present calculation is an extension into the nonlinear regime of the work of Hall, Malik & Poll (1984). Hereafter, we refer to that paper as I, and we shall shortly discuss the relevant details of that paper. The linear theory given in I was motivated

† Research was supported by the National Aeronautics and Space Administration under NASA Contract No. NAS1-17070 while this author was in residence at ICASE, NASA Langley Reaearch Center, Hampton, VA 23665.

‡ Research was supported by the National Aeronautics and Space Administration under NASA Contract No. NAS1-16916 while this author was employed at High Technology Corporation, PO Box 7262, Hampton, VA 23666.

by the experimental investigations of Pfenninger & Bacon (1969) and Poll (1979, 1980). These authors measured the frequencies of naturally occurring disturbances along the attachment lines of the flows over different swept cylinders. It was found that small-amplitude time-periodic disturbances exist above a certain critical Reynolds number and correspond to the lower branch of the neutral curve calculated in I. None of the experimental points appeared to correspond to upper-branch disturbances; however, it is, of course, possible that, if the flow were forced by, for example, a vibrating ribbon, then such modes might be observed. The first aim of the present study is to determine whether a weakly nonlinear stability calculation based on the Stuart–Watson expansion procedure can explain why the flow exhibits a preference for lower-branch modes. We show that, apart from a small interval near the critical Reynolds number, finite-amplitude solutions bifurcate subcritically from the upper branch. This means that these solutions are unstable and therefore would not correspond to an observable equilibrium state. However, the existence of these solutions suggests that the basic state might be nonlinearly unstable to sufficiently large finite-amplitude disturbances. For this reason we decided to investigate numerically the full nonlinear stability equations using a Fourier–Chebyshev expansion to represent the spatial structure of the disturbance flowfield.

In fact, Pfenninger & Bacon found that turbulence wires introduced into the attachment region could induce large-amplitude disturbances in the boundary layer at Reynolds numbers significantly below the linear critical point. Thus we use a Fourier–Chebyshev spectral method to simulate finite-amplitude disturbances at Reynolds numbers not necessarily close to the neutral curve. In recent years similar calculations for flows such as plane Poiseuille flow have become commonplace, and the reader is referred to, for example, the papers by Orszag & Kells (1980) and Moin & Kim (1982). This type of calculation follows the time evolution of an initial perturbation imposed on the basic flow, so that unstable time-periodic equilibrium states of the type calculated by Herbert (1977) cannot be found by this approach. However, the size of such periodic disturbances can be inferred if required by gradually increasing the size of the initial perturbation.

In order to check the results of our calculations, we shall compare the numerical results with those predicted by weakly nonlinear stability theory. In particular, we calculate numerically the supercritically bifurcating solutions close to the lower branch and see how the size of the equilibrated disturbance compares with that predicted by the Stuart–Watson method. Further checks are made by comparing our numerical results for small-amplitude disturbances with the results of I. We shall show that below the linear critical Reynolds number it is possible to induce nonlinearly unstable perturbations by appropriate choices of the wavenumber and the initial amplitude of the disturbance. Qualitatively we shall find that our results are consistent with the available experimental results. It is possible that the quantitative agreement between theory and experiment which we find in the weakly nonlinear regime cannot be reproduced in the fully nonlinear regime because the disturbances produced experimentally by Pfenninger & Bacon were necessarily three-dimensional. The procedure adopted in the rest of the paper is as follows: In §2 we formulate the stability equations which govern the stability of the three-dimensional boundary layer obtained by introducing a crossflow into the classical Hiemenz boundary-layer solution. In §3 we discuss the instability in the weakly nonlinear regime whilst in §4 we discuss the numerical simulation of large-amplitude disturbances. Finally, in §5 we discuss our results and their practical implications.

2. Formulation of the problem

Let us consider the flow of a viscous fluid of kinematic viscosity ν over the flat plate defined by $y = 0$. The velocity of the fluid with respect to the Cartesian coordinate system (x, y, z) is (u, v, w), and sufficiently far away from the plate

$$u \sim U_e \frac{x}{l}, \quad w \sim W_e, \tag{2.1}$$

whilst at the wall we impose the conditions

$$u = w = 0, \quad v = V_e. \tag{2.2}$$

We define Δ, R, and κ by

$$\Delta = \left(\frac{\nu l}{U_e}\right)^{\frac{1}{2}}, \quad R = \frac{W_e \Delta}{\nu}, \quad \kappa = V_e \left\{\frac{l}{\nu U_e}\right\}^{\frac{1}{2}}, \tag{2.3a, b, c}$$

so that Δ is the thickness of the boundary layer at the wall whilst R and κ are the Reynolds number and a non-dimensional suction parameter, respectively.

It is convenient to diverge from the scalings of I and write

$$\boldsymbol{u} = W_e \bar{\boldsymbol{U}}(X, Y, Z, t), \quad p = \rho W_e^2 \bar{P}(X, Y, Z, t), \tag{2.4}$$

where ρ is the fluid density whilst $(X, Y, Z) = \Delta^{-1}(x, y, z)$ and the time variable t has been scaled on ΔW_e^{-1}. The continuity and momentum equations then take the form

$$\nabla \cdot \bar{\boldsymbol{U}} = 0, \quad \bar{\boldsymbol{U}}_t + (\bar{\boldsymbol{U}} \cdot \nabla)\, \bar{\boldsymbol{U}} = -\nabla \bar{P} + \frac{1}{R} \nabla^2 \bar{\boldsymbol{U}}, \tag{2.5a, b}$$

and when $Y \to \infty$ we require that $U \to X/R$, $W \to 1$. We therefore choose to seek a solution of (2.5) which has the particular structure

$$\bar{\boldsymbol{U}} = (XU, V, W), \quad \bar{P} = -\frac{X}{R^2} + P, \tag{2.6}$$

where U, V, W and P now depend only on Y, Z and t. The equations (2.5) then simplify to

$$\left.\begin{aligned} U + V_Y + W_Z &= 0, \\ U_t + U^2 + VU_Y + WU_Z &= \frac{1}{R^2} + \frac{1}{R}\{U_{YY} + U_{ZZ}\}, \\ V_t + VV_Y + WV_Z &= -P_Y + \frac{1}{R}\{V_{YY} + V_{ZZ}\}, \\ W_t + VW_Y + WW_Z &= -P_Z + \frac{1}{R}\{W_{YY} + W_{ZZ}\}, \end{aligned}\right\} \tag{2.7}$$

which are to be solved subject to

$$\left.\begin{aligned} U = W = 0, \quad V = \frac{\kappa}{R}, \quad Y = 0; \\ U \to \frac{1}{R}, \quad W \to 1, \quad Y \to \infty. \end{aligned}\right\} \tag{2.8}$$

In the absence of any disturbance, the basic flow takes the form

$$U = \frac{1}{R}\bar{u}(Y), \quad V = \frac{1}{R}\bar{v}(Y), \quad W = \bar{w}(Y),$$

where $\bar{u}$, $\bar{v}$, and $\bar{w}$ are determined by solving

$$\left.\begin{aligned} &\bar{u}+\bar{v}' = 0, \\ &\bar{v}'''+\bar{v}'^2-\bar{v}\bar{v}''-1 = 0, \\ &\bar{w}''-\bar{v}\bar{w}' = 0, \\ &\bar{v}'(0) = 0, \quad \bar{v}(0) = \kappa, \quad \bar{v}'(\infty) = -1, \quad \bar{w}(0) = 0, \quad \bar{w}(\infty) = 1. \end{aligned}\right\} \tag{2.9}$$

When the disturbance imposed on the flow is not small, we must solve (2.7) subject to (2.8) numerically, and this will be discussed in §4. When the disturbance is sufficiently small for us to use weakly nonlinear stability theory based on the Stuart–Watson method, it is convenient for us to write

$$U = \frac{\bar{u}}{R}+\tilde{U}, \quad V = \frac{\bar{v}}{R}+\tilde{V}, \quad W = \bar{w}+\tilde{W}, \tag{2.10}$$

in which case $\tilde{U}$, $\tilde{V}$, $\tilde{W}$ and P satisfy

$$\left.\begin{aligned} &\tilde{U}+\tilde{V}_Y+\tilde{W}_Z = 0, \\ &\mathscr{L}\tilde{U}-\{2\bar{u}\tilde{U}+\tilde{V}\bar{u}'\} = R\{\tilde{U}^2+\tilde{V}\tilde{U}_Y+\tilde{W}\tilde{U}_Z\}, \\ &\mathscr{L}\tilde{V}-V\bar{v}' = RP_Y+R\{\tilde{V}\tilde{V}_Y+\tilde{W}\tilde{V}_Z\}, \\ &\mathscr{L}\tilde{W}+R\tilde{V}\bar{w}' = RP_Z+R\{\tilde{V}\tilde{W}_Y+\tilde{W}\tilde{W}_Z\}. \end{aligned}\right\} \tag{2.11}$$

Here the operator $\mathscr{L}$ is defined by

$$\mathscr{L} \equiv \frac{\partial^2}{\partial Y^2}+\frac{\partial^2}{\partial Z^2}-R\frac{\partial}{\partial t}-R\bar{w}\frac{\partial}{\partial Z}-\bar{v}\frac{\partial}{\partial Y}. \tag{2.12}$$

The discussion of I was restricted to the linear regime where the nonlinear terms in (2.11) can be neglected; in the following section we determine how these disturbances develop in a neighbourhood of the neutral curve, whilst in §4 larger disturbances will be calculated by integrating (2.7) numerically.

3. Weakly nonlinear stability theory

In I the solution of the linearized version of (2.12) was discussed. This was done by taking $\tilde{U}$, $\tilde{V}$, $\tilde{W}$ and P to be proportional to $E = \exp(\mathrm{i}\alpha[Z-ct])$. Thus the disturbance has wavelength $2\pi/\alpha$ and propagates along the attachment line with speed c. We found in I that in the case of zero suction instability is possible for $R > 583.1$ and that with suction the flow is significantly stabilized. We follow the usual approach of weakly nonlinear stability theory and determine how the disturbance develops in a neighbourhood of a point on the neutral curve in the (α, R)-plane. Suppose then that (α_0, R_0) is a point on a neutral curve for some values of κ and that the corresponding value of c is c_0. We expand

$$R = R_0+\epsilon R_1+\ldots, \tag{3.1}$$

where $0 < \epsilon \ll 1$ and define a slow time variable τ by

$$\tau = \epsilon t. \tag{3.2}$$

The X velocity component then expands as

$$\tilde{U} = \{\epsilon^{\frac{1}{2}}\tilde{U}_0 E+\epsilon\tilde{U}_2 E^2+\epsilon^{\frac{3}{2}}\tilde{U}_3 E^3+\epsilon^{\frac{3}{2}}\tilde{U}_4 E\}+\text{c.c.}+\epsilon\tilde{U}_M+O(\epsilon^2)$$

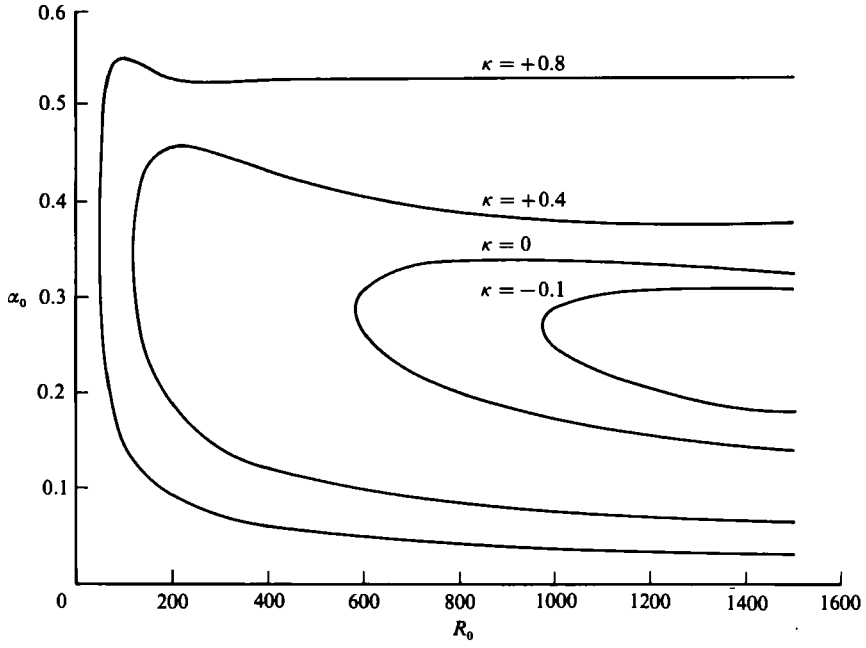

FIGURE 1. The neutral curves in the (α_0, R_0)-plane for different values of κ.

where c.c. is the complex conjugate and $\tilde{V}$, $\tilde{W}$ and P are expanded in a similar manner. It is then a routine procedure to substitute the above expansions into (2.12) and equate like powers of $\epsilon^{\frac{1}{2}}$. At order $\epsilon^{\frac{1}{2}}$ we find that

$$(\tilde{U}_0, \tilde{V}_0) = A(\tau)\,(U_0, V_0),$$

where $A(\tau)$ is an amplitude function to be determined at higher order whilst (U_0, V_0) satisfies the sixth-order differential system

$$\left.\begin{aligned} &\{\mathrm{M}_1 + \mathrm{i}\alpha_0 R_0 c_0\}\, U_0 - 2\bar{u}U_0 - \bar{u}'V_0 - \bar{v}U_0' - \mathrm{i}\alpha_0 R_0 \bar{w} U_0 = 0, \\ &\{\mathrm{M}_1 + \mathrm{i}\alpha_0 R_0 c_0\}\,\mathrm{M}_1 V_0 - \mathrm{i}\alpha_0 R_0 \bar{w}\mathrm{M}_1 V_0 + \mathrm{i}\alpha_0 R_0 \bar{w}'' V_0 \\ &\qquad - \bar{v}\mathrm{M}_1 V_0' - \bar{v}'\mathrm{M}_1 V_0 + 2\bar{u}'U_0 + 2\bar{u}U_0' + \bar{u}''V_0 + \bar{u}'V_0' = 0, \\ &\qquad U_0 = V_0 = V_0' = 0, \quad Y = 0, \infty, \end{aligned}\right\} \tag{3.3}$$

where $\mathrm{M}_j \equiv \mathrm{d}^2/\mathrm{d}Y^2 - \alpha_0^2 j^2$. Thus (3.3) is just the eigenvalue problem discussed in I, and in figures 1 and 2 we have shown the neutral values of α_0, $\alpha_0 c_0$ for several different values of κ. The eigenrelation was obtained by using a fourth-order-accurate finite-difference scheme to solve (3.3) after first writing $\boldsymbol{V} = [V_0, V_0', V_0'', V_0''', U_0, U_0']^{\mathrm{T}}$, so that $\boldsymbol{V}$ satisfies an equation of the form

$$\frac{\mathrm{d}\boldsymbol{V}}{\mathrm{d}Y} = \boldsymbol{B}\boldsymbol{V}, \tag{3.4}$$

where $\boldsymbol{B}$ is a 6×6 matrix whose elements are given explicity in I. Later we shall need the solution of the system adjoint to (3.3), and if $\boldsymbol{q} = [q_1, q_2, q_3, q_4, q_5, q_6]^{\mathrm{T}}$ is the adjoint vector, the appropriate system is

$$\frac{\mathrm{d}\boldsymbol{q}}{\mathrm{d}Y} = -\boldsymbol{B}^{\mathrm{T}}\boldsymbol{q}, \quad q_3 = q_4 = q_6 = 0, \quad Y = 0, \infty. \tag{3.5}$$

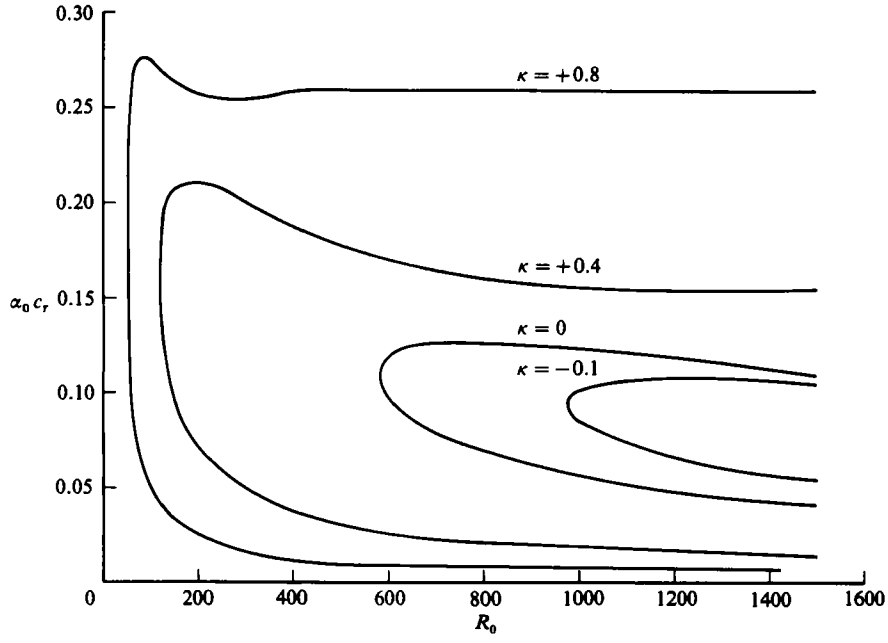

FIGURE 2. The neutral curves in the $(\alpha_0 c_0, R_0)$-plane for different values of κ.

Here the precise manner in which these functions decay to zero can be found by looking at the asymptotic solution of the adjoint differential equation for $Y \gg 1$. We note here only that, if we insist that this decay is exponential, then (3.5) has only a discrete spectrum of eigenvalues which, of course, is identical with that associated with (3.3).

At order ϵ we find that

$$(\tilde{U}_2, \tilde{V}_2) = A^2(U_2, V_2), \quad (\tilde{U}_M, \tilde{V}_M, \tilde{W}_M, \tilde{P}_M) = |A|^2 (U_M, V_M, W_M, P_M),$$

where (U_2, V_2) satisfy

$$\left.\begin{aligned} &\{\mathrm{M}_2 + 2\mathrm{i}\alpha_0 R_0 c_0\} U_2 - 2\bar{u} U_2 - \bar{u}' V_2 - \bar{v} U_2' - 2\mathrm{i}\alpha_0 R_0 \bar{w} U_2 = R_0\{V_0 U_0' - U_0 V_0'\}, \\ &\{\mathrm{M}_2 + 2\mathrm{i}\alpha_0 R_0 c_0\} \mathrm{M}_2 V_2 - 2\mathrm{i}\alpha_0 R_0 \bar{w} \mathrm{M}_2 V_2 + \mathrm{i}\alpha_0 R_0 \bar{w}'' V_2 - \bar{v} \mathrm{M}_2 V_2' \\ &\quad = -R_0[-4\alpha_0^2 U_0 V_0 + 2(2U_0 U_0' + V_0' V_0'' + U_0' V_0' - V_0 V_0''' - V_0 U_0'' + 2U_0 V_0'')], \end{aligned}\right\} \tag{3.6}$$

whilst the mean-flow correction is determined by

$$U_M + V_M' = 0, \tag{3.7a}$$

$$U_M'' - \bar{v} U_M' - 2\bar{u} U_M - V_M \bar{u}' = R_0\{4|U_0|^2 + (V_0 U_0^*)' + (V_0^* U_0)'\}, \tag{3.7b}$$

$$V_M'' - \bar{v} V_M' - V_M \bar{v}' - R_0 P_M' = R_0\{2(V_0 V_0^*)' + U_0 V_0^* + U_0^* V_0\}, \tag{3.7c}$$

$$W_M'' - \bar{v} W_M' - R_0 V_M \bar{w}' = \frac{R_0}{\mathrm{i}\alpha_0}\{V_0 U_0^{*\prime} + V_0 V_0^{*\prime\prime} - V_0^* U_0' - V_0'' V_0^*\}, \tag{3.7d}$$

where $*$ denotes complex conjugate. The system of equations (3.6) is to be solved subject to

$$U_2 = V_2 = V_2' = 0, \quad Y = 0,$$

with U_2, V_2 tending to zero exponentially when $Y \to \infty$. Now turning to the mean-field correction equations, we note that U_M can be eliminated from (3.7*b*) using the

equation of continuity to give a third-order equation for V_M. For large values of Y this equation has the three independent solutions

$$V_M \sim \text{constant},$$
$$V_M \sim Y^3,$$
$$V_M \sim \mathrm{e}^{-\frac{1}{2}Y^2},$$

so that, in order to satisfy the no-slip condition $V_M = U_M = 0$ at the wall, we relax the condition on V_M at infinity to

$$V'_M \to 0, \quad Y \to \infty. \tag{3.8}$$

Having determined V_M, we can then integrate (3.7*d*) to find W_M and we note that the structure of the equation for W_M for $Y \gg 1$ enables us to find a W_M such that

$$W_M(0) = 0, \quad W_M \to 0 \text{ (exponentially)}, \quad Y \to \infty. \tag{3.9}$$

Finally, U_M and P_M can then be determined from (3.7*a*, *c*) respectively.

At order $\epsilon^{\frac{3}{2}}$ we obtain differential systems for $(\bar{U}_3, \bar{V}_3, \bar{W}_3, \bar{P}_3)$, $(\bar{U}_4, \bar{V}_4, \bar{W}_4, \bar{P}_4)$, in the usual way. We obtain an amplitude equation for $A(\tau)$ as a solvability condition on the system for $(\bar{U}_3, \bar{V}_3, \bar{W}_3, \bar{P}_3)$. The equation takes the form

$$\frac{\mathrm{d}A}{\mathrm{d}\tau} = a_0 R_1 A + a_1 A |A|^2, \tag{3.10}$$

where the constants a_0 and a_1 are defined by

$$a_0 = \frac{-\int_0^\infty [\mathrm{i}\alpha_0 \{(\bar{w} - c_0)(V_0'' - \alpha_0^2 V_0) + \bar{w}'' V_0\} q_4 + \mathrm{i}\alpha_0 \{(\bar{w} - c_0) U_0\} q_6] \,\mathrm{d}Y}{R_0 \int_0^\infty [U_0 q_6 + (V_0'' - \alpha_0^2 V_0) q_4] \,\mathrm{d}Y}, \tag{3.11a}$$

$$\begin{aligned} a_1 \int_0^\infty & [U_0 q_6 + (V_0'' - \alpha_0^2 V_0) q_4] \,\mathrm{d}Y \\ &= -\int_0^\infty R_0 [q_4 \{-\alpha_0^2 (V_0 V'_M + V_M V'_0 + \mathrm{i}\alpha_0 W_M V_0 + 3 V_2 V_0^{*\prime} + \tfrac{3}{2} V_0^* V'_2 \\ &\quad + 2 V_2 U_0^* + \tfrac{1}{2} U_2 V_0^*) - \mathrm{i}\alpha_0 (V_0 W''_M - W_M U'_0 - W'_M U_0 - W_M V''_0) \\ &\quad + \tfrac{1}{2}(2 V_0^{*\prime} U'_2 + V_0^* U''_2 + V_0^* V'''_2 + 2 V_0^{*\prime} V''_2 + 2 V'_M U'_0 + 2 V_M U''_0 \\ &\quad + 2 V'_M V''_0 + 2 V_M V'''_0 - 2 V_2 U_0^{*\prime\prime} - V'_2 U_0^{*\prime} - 2 V_2 V_0^{*\prime\prime\prime} - V'_2 V_0^{*\prime\prime} \\ &\quad + U_2 U_0^{*\prime} + U'_2 U_0^* + U_2 V_0^{*\prime\prime} + U_0^* V''_2)\} + q_6 \{\mathrm{i}\alpha_0 W_M U_0 + V_M U'_0 + V_0 U'_M \\ &\quad + 2 U_0 U_M + \tfrac{3}{2} U_0^* U_2 + V_0^* U'_2 + \tfrac{1}{2} U_0^* V'_2 + U_0^* V_2 + 2 U_2 V_0^{*\prime}\}] \,\mathrm{d}Y. \end{aligned} \tag{3.11b}$$

The constants a_0 and a_1 can be determined only after integrating numerically the differential systems for the eigenfunction, adjoint eigenfunction, first-harmonic function and the mean-field correction. This was done using the fourth-order accurate finite-difference scheme described in I. In all the calculations the eigenfunctions were normalized such that the maximum value of $|W_0|$ was unity. The integrals appearing in the definition of a_0 and a_1 were then evaluated using the trapezium rule; the results of a calculation for $\kappa = -0.1, 0, 0.4, 0.8$ are shown in figure 3. We have only given results for the real parts of a_0 and a_1 since this information is sufficient to calculate

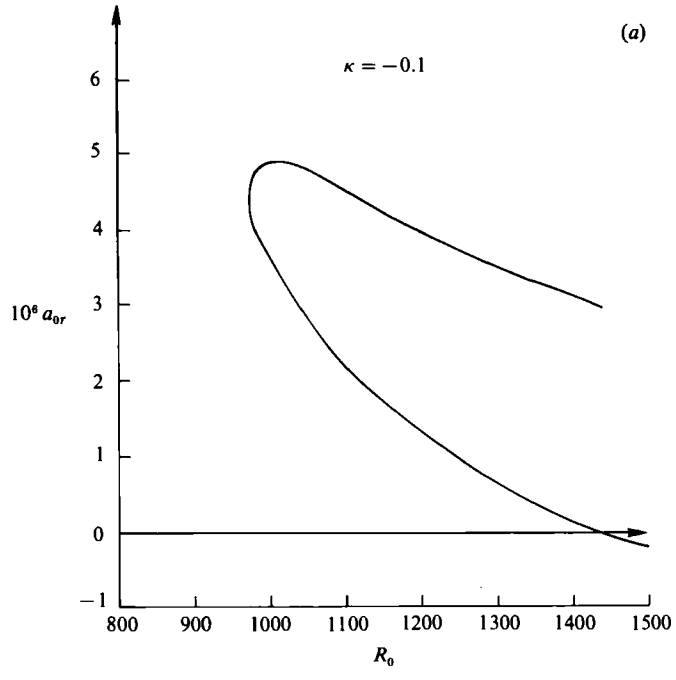

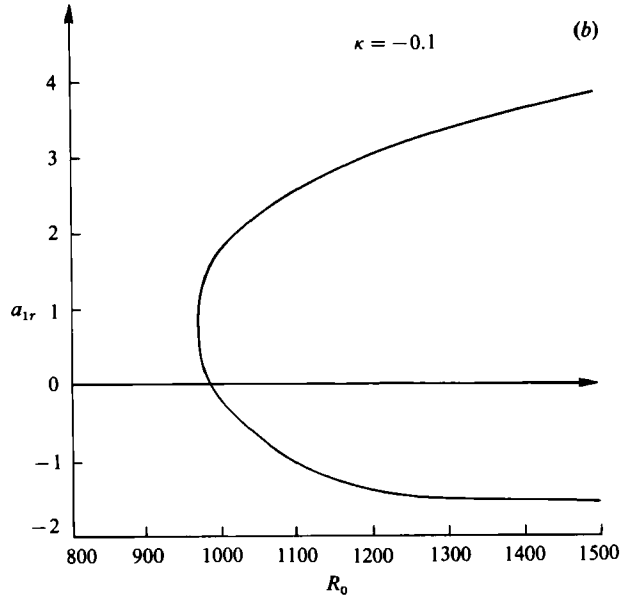

FIGURE 3(a,b). For caption see p. 267.

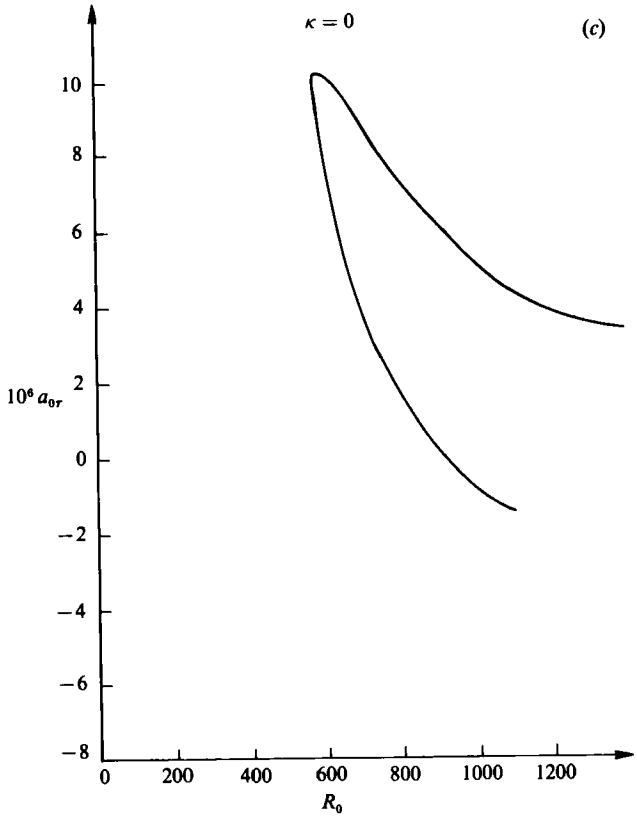

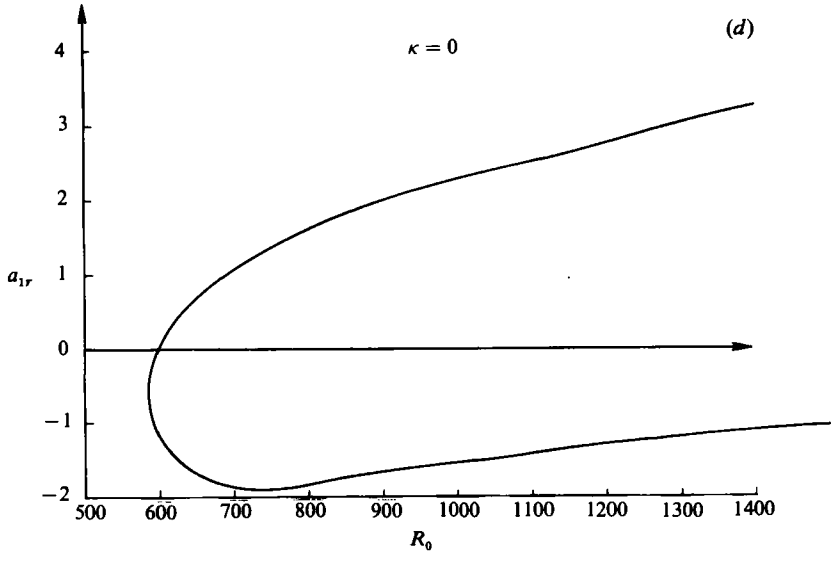

FIGURE 3(*c*,*d*). For caption see p. 267.

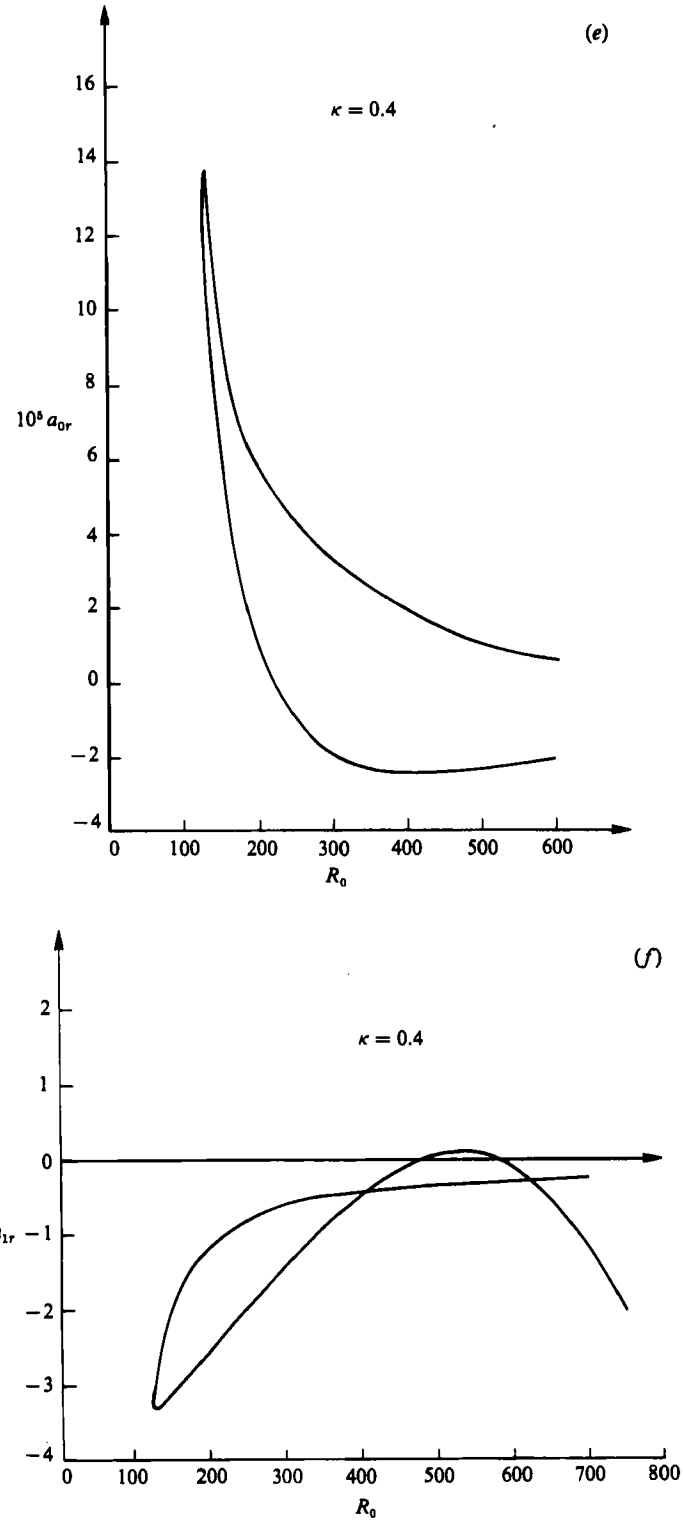

FIGURE 3(e,f). For caption see p. 267.

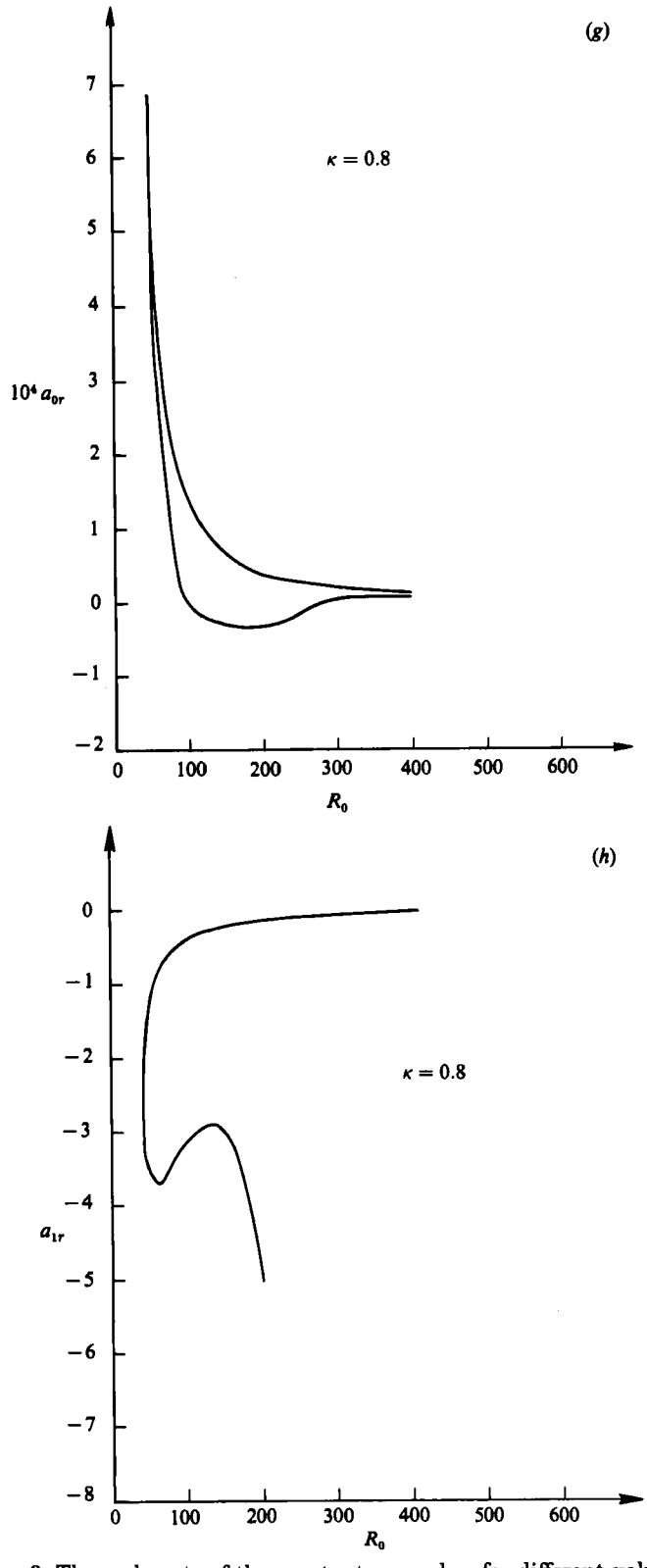

FIGURE 3. The real parts of the constants a_0 and a_1 for different values of κ.

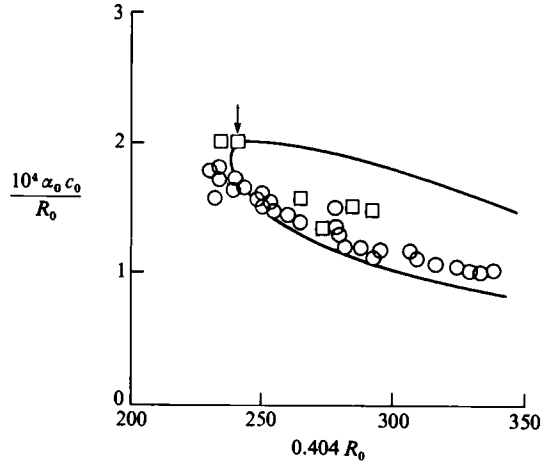

FIGURE 4. Comparison of the calculated neutral curve with the experiment. The finite-amplitude solution bifurcates subcritically beyond the arrow marked along the upper branch. ○, Pfenninger & Bacon (1969); □, Poll (1979, 1980).

the amplitude of an equilibrium disturbance. Before discussing these results further we note from (3.10) that

$$\frac{1}{2}\frac{\mathrm{d}}{\mathrm{d}\tau}|A|^2 = R_1 a_{0r}|A|^2 + a_{1r}|A|^4,$$

so that equilibrium solutions are possible if

$$|A|^2 = -R_1 a_{0r} a_{1r}^{-1},$$

and this solution is stable if the bifurcation is supercritical ($a_{1r} < 0$) and unstable if the bifurcation is subcritical ($a_{1r} > 0$). In the latter case a finite-amplitude motion having $|A|^2 > R_1 a_{0r} a_{1r}^{-1}$ causes $|A|$ to increase without limit.

Now let us turn to the results illustrated in figure 3. The most important results correspond to $\kappa = 0$, and we see that the bifurcation is always supercritical on the lower branch. But a_{1r} has a zero near $R_0 \approx 595$, and for the remainder of the upper branch the bifurcation is subcritical. In figure 4 we have shown the neutral curve for $\kappa = 0$ together with the experimental points due to Poll (1979, 1980) and Pfenninger & Bacon (1969). We have marked by an arrow the position along the upper branch beyond which the finite-amplitude solution bifurcates subcritically and is unstable. As expected, it seems that the experiments have picked up the disturbances corresponding to the parts of the neutral curve where the bifurcation is supercritical. Later we shall describe a numerical investigation of finite-amplitude disturbances, and in order to test our calculations we shall try to reproduce quantitatively the finite-amplitude solution which bifurcates supercritically from the lower branch at $R_0 = 800$. We shall also investigate the possibility of finite-amplitude motions at Reynolds numbers significantly less than the critical value. These disturbances are to be expected since the bifurcation is subcritical over most of the upper branch.

It remains for us to discuss the results for the cases when $\kappa \neq 0$. We see that increasing the blowing at the wall reduces the Reynolds-number regime over which subcritical disturbances are possible. In fact when $\kappa = 0.8$ the bifurcation is always supercritical so that the flow is not susceptible to 'threshold amplitude' effects.

We see in figure 3 that when $\kappa = -0.1$ the point on the neutral curve where there is a crossover from subcritical to supercritical bifurcation moves down from the upper branch to a point on the lower branch. Thus, the bifurcation is now subcritical at

the critical Reynolds number. This is consistent with the results of Hocking (1974) who investigated the nonlinear stability of the asymptotic suction boundary layer which corresponds to the limit $\kappa \to -\infty$. Furthermore, we note that at some values of κ in this range $(-0.1, 0)$ the zero of a_{1r} must occur at the critical Reynolds number; thus, if we wanted to extend our analysis to include slow spanwise variations the appropriate evolution equation would not in this case be that found by Stewartson & Stuart (1971) and would have to include fifth-order terms in the disturbance amplitude.

The evolution of the supercritically bifurcating solution with increasing Reynolds number is beyond the scope of the present calculation. However, if the disturbances develop in a manner typical of convective or centrifugal instabilities, it is possible that the flow remains laminar over a significant range of values of the Reynolds number. If three-dimensional instabilities of the supercritically bifurcating solution exist then the subsequent development of the flow would be more complex. However, if the origin of transition on the attachment line of a swept wing is due to subcritical disturbances, then it is not clear whether suction would be effective in keeping the attachment line stable. This follows from the fact that suction, although increasing the critical Reynolds number, makes the flow more susceptible to subcritical disturbances. In contrast, blowing ultimately causes the disappearance of subcritical disturbances but lowers the critical Reynolds numbers at which infinitesimal disturbances are unstable.

4. Direct numerical simulation

The attachment-line boundary layer is strictly parallel; i.e. the basic flow is independent of the coordinate along the attachment line. Therefore we can employ periodic boundary conditions in that direction for the solution of (2.7). This is to be contrasted with the Blasius boundary layer, where periodic boundary conditions do not simulate the actual physical problem in a rational way, as the growth of the boundary layer cannot be accounted for.

For the present boundary layer, a Fourier–Chebyshev spectral method will be used to simulate two-dimensional finite-amplitude states. We use the spectral-collocation method of Malik, Zang & Hussaini (1984) (hereafter referred to as MZH) for the solution of (2.7) subject to the boundary conditions (2.8). A stretching transformation can be applied in the (unbounded) vertical direction. Let

$$Y = a\frac{1+\eta}{b-\eta}, \tag{4.1}$$

where Y is the physical vertical coordinate, η the computational coordinate and a and b are constants. Let $Y_{\max}$ be the upper boundary in the physical plane and set

$$b = 1 + \frac{2a}{Y_{\max}}. \tag{4.2}$$

Then for any choice of the scaling parameter a, the computational coordinate η falls within the standard Chebyshev interval $[-1, 1]$. The collocation points in the computional plane are

$$Z_j = j\frac{L_Z}{K}, \quad j = 0, 1, \ldots, K-1, \tag{4.3}$$

$$\eta_m = \cos\frac{m\pi}{N}, \quad m = 0, 1, \ldots, N, \tag{4.4}$$

where $L_Z = 2\pi/\alpha$, and K and N are the number of intervals in the Z and Y directions, respectively. The dependent variables have Fourier–Chebyshev series of the form

$$u(Z, Y, t) = \sum_{k=-\frac{1}{2}K}^{\frac{1}{2}K-1} \sum_{n=0}^{N} u_{kn}(t)\, e^{2\pi i k Z/L_Z}\, T_n(\eta), \tag{4.5}$$

where T_n is the Chebyshev polynominal of degree n. In the spectral collocation method, spatial derivatives of u are obtained by differentiating the series expansion with the expansion coefficients $u_{kn}(t)$ determined by discrete Fourier and Chebyshev transforms of the grid-point values of u. The details of the procedure are given in Gottlieb & Orszag (1977). Derivatives in the vertical direction are evaluated by multiplying the Chebyshev collocation in η by the Jacobian of the transformation, i.e.

$$u_Y = \frac{d\eta}{dY} u_\eta. \tag{4.6}$$

In the temporal discretization, the pressure-gradient term and the incompressibility constraint are best handled implicitly. So, too, are the vertical diffusion terms because of the fine mesh-spacing near the wall. We use Crank–Nicholson time discretization on the implicit terms and second-order Adams–Bashforth on the remainder. After a discrete Fourier transform in Z, the following set of ordinary differential equations results (we list them in the order they are stacked for numerical computations):

$$\left.\begin{aligned} -\hat{U}^{n+1} - \hat{V}_Y^{n+1} - i\hat{k}\hat{W}^{n+1} &= 0, \\ -\beta\hat{V}_{YY}^{n+1} + \hat{V}^{n+1} + \hat{Q}_Y^{n+1} &= \hat{V}^n + \tfrac{1}{2}\Delta t(3\hat{H}_1^n - \hat{H}_1^{n-1}) - \hat{Q}_Y^n + \beta\hat{V}_{YY}^n, \\ -\beta\hat{W}_{YY}^{n+1} + \hat{W}^{n+1} + i\hat{k}\hat{Q}^{n+1} &= \hat{W}^n + \tfrac{1}{2}\Delta t(3\hat{H}_2^n - \hat{H}_2^{n-1}) - i\hat{k}\hat{Q}^n + \beta\hat{W}_{YY}^n, \\ -\beta\hat{U}_{YY}^{n+1} + \hat{U}^{n+1} &= \hat{U}^n + \tfrac{1}{2}\Delta t(3\hat{H}_3^n - \hat{H}_3^{n-1}) + \beta\hat{U}_{YY}^n. \end{aligned}\right\} \tag{4.7}$$

In the above, $\hat{k} = 2\pi k/L_Z$, $\beta = \Delta t/2R$, $\hat{Q} = \frac{1}{2}\Delta t\hat{P}$, $i = (-1)^{\frac{1}{2}}$, and $\hat{}$ denotes Fourier-transformed variables in wavenumber space. The wavenumber is denoted by $\hat{k}$ and the dependence of $\hat{W}$, $\hat{V}$, $\hat{Q}$ and $\hat{U}$ (the order of the dependent variables here represents that of the solution vector adopted for the numerical solution of (4.7)) upon $\hat{k}$ has been suppressed. The superscript n represents the time level. H_1, H_2 and H_3, which contain the terms treated explicitly, are given by

$$\left.\begin{aligned} H_1 &= -VV_Y - WV_Z + \frac{1}{R}V_{ZZ}, \\ H_2 &= -VW_Y - WW_Z + \frac{1}{R}W_{ZZ}, \\ H_3 &= -VU_Y - WU_Y + \frac{1}{R}U_{ZZ} - U^2 + \frac{1}{R^2}. \end{aligned}\right\} \tag{4.8}$$

Appropriate boundary conditions are yet to be prescribed for (4.7), and will be discussed later.

For each wavenumber $\hat{k}$, the system of equations (4.7) can be written as

$$\boldsymbol{L}\boldsymbol{S} = \boldsymbol{F}, \tag{4.9}$$

where $\boldsymbol{S} = [\hat{W}^{n+1}, \hat{V}^{n+1}, \hat{Q}^{n+1}, \hat{U}^{n+1}]$ and $\boldsymbol{F}$ is the known right-hand side. The matrix $\boldsymbol{L}$ constructed by using Chebyshev polynomials is a full $M \times M$ matrix where $M \approx 4N$. A direct solution of (4.9) by Gauss elimination methods would require $O(M^2)$ storage

and $O(M^3)$ arithmetic operations. In the present study, we use a spectral iteration scheme, based on a minimum residual (MR) method with finite-difference preconditioning, that requires only $O(M)$ storage and $O(M \log M)$ operations per iteration. An effective preconditioning is provided by using a staggered mesh in the normal direction, whereby the velocities are defined at the cell faces η_m, and the pressure at the cell centres

$$\eta_{m-\frac{1}{2}} = \cos\left(\pi \frac{m-\frac{1}{2}}{N}\right), \quad m = 1, 2, \ldots, N. \tag{4.10}$$

The momentum equations are enforced at the cell faces, whereas the continuity equations are enforced at the centres. More details of the iterative spectral method employing staggered mesh are given in MZH.

We how return to the question of boundary conditions imposed for the numerical solution of (4.7). Because of the staggered mesh in the vertical direction, no artificial pressure boundary conditions are required. The velocity boundary conditions for $\hat{k} \neq 0$ are

$$\left.\begin{aligned} &\hat{U} = \hat{V} = \hat{W} = 0, \quad Y = 0, \\ \text{and} \quad &\hat{U} = \hat{V} = \hat{W} = 0, \quad Y = Y_{\max}, \end{aligned}\right\} \tag{4.11}$$

$$\text{or} \qquad \hat{U}_Y = -Y_{\max}\hat{U}, \quad \hat{V}_Y = -|\hat{k}|\hat{V}, \quad \hat{W}_Y = -|\hat{k}|\hat{W}, \quad Y = Y_{\max}.$$

In some test runs, both the zeroth-order and first-order boundary conditions at $Y = Y_{\max}$ gave almost identical results when $Y_{\max} \geqslant 15$. With the first-order boundary conditions, the iteration scheme (MR) converged faster; and, therefore, these conditions were imposed at $Y_{\max} = 15$ in all the calculations to be reported in this section. This fast convergence with first-order boundary conditions was also noted in MZH.

For $\hat{k} = 0$, the boundary conditions are

$$\left.\begin{aligned} &\hat{V} = \frac{\kappa}{R}, \quad \hat{W} = \hat{U} = 0, \quad Y = 0, \\ &\hat{W} = 1, \quad \hat{U} = \frac{1}{R}, \quad Y = Y_{\max}. \end{aligned}\right\} \tag{4.12}$$

The structure of (4.7) for $\hat{k} = 0$, with the above boundary conditions, is quite simple. In this case $\hat{W}$ and $\hat{U}$ satisfy two tridiagonal equations, and after first solving this system the continuity equation is then solved as a bidiagonal equation for $\hat{V}$. Once $\hat{V}$ is known, the pressure $\hat{Q}$ also satisfies a bidiagonal equation. This is solved by setting $\hat{Q}(Y_{\frac{1}{2}}) = 0$ and then solving for each successive value of the pressure. This particular choice of $\hat{Q}(Y_{\frac{1}{2}})$ is arbitrary and corresponds to specifying the mean pressure.

Initial conditions required for the solution of (4.7) are provided by imposing a disturbance of finite amplitude upon the basic state. The disturbance eigenfunctions are calculated using linear theory as discussed in I. The initial conditions thus are

$$\left.\begin{aligned} U(Z, Y, 0) &= \frac{\bar{u}(y)}{R} + \epsilon\,\mathrm{Re}\{U_0(Y)\,\mathrm{e}^{\mathrm{i}\alpha Z}\}, \\ V(Z, Y, 0) &= \frac{\bar{v}(Y)}{R} + \epsilon\,\mathrm{Re}\{V_0(Y)\,\mathrm{e}^{\mathrm{i}\alpha Z}\}, \\ W(Z, Y, 0) &= \bar{w}(Y) + \epsilon\,\mathrm{Re}\{W_0(Y)\,\mathrm{e}^{\mathrm{i}\alpha Z}\}, \end{aligned}\right\} \tag{4.13}$$

where the disturbance eigenfunctions U_0, V_0, W_0 have been normalized such that the maximum value is 1. The parameter ϵ has been introduced to control the magnitude of initial disturbance.

Let us define the flow energy at any time t as

$$E(t) = \int_0^{L_Z} \mathrm{d}Z \int_0^{Y_{\max}} \left\{ \left(U(Z, Y, t) - \frac{\bar{u}}{R} \right)^2 + \left(V(Z, Y, t) - \frac{\bar{v}}{R} \right)^2 + (W(Z, Y, t) - \bar{w})^2 \right\} \mathrm{d}Y \tag{4.14}$$

and rate of change of the disturbance amplitude as

$$\sigma = \frac{1}{2E} \frac{\mathrm{d}E}{\mathrm{d}t}, \tag{4.15}$$

where $\sigma > 0$ and $\sigma < 0$ signify growing and decaying disturbances respectively.

In the numerical calculations which are reported below, we have used 33 Chebyshev polynomials in the normal direction whilst the number of Fourier modes along the attachment line varies from case to case. Excellent agreement between the numerical results and linear theory was achieved in MZH for plane Poiseuille flow and Blasius boundary layer with only 33 Chebyshev polynomials. We compared the solution of (4.7) with linear theory results just to check the accuracy of the numerical scheme and found satisfactory agreement. As a example, calculations were performed at $\alpha = 0.25648$ for three different Reynolds numbers using $\epsilon = 0.0001$ and $K = 4$. The results are presented in table 1. These results were obtained using a time step $\Delta t = CFL\,(L_Z/K)$ with a CFL number of 0.1. Calculations were terminated at $t = 306$, which corresponds to about 4.5 linear wave periods. For all three Reynolds numbers, the difference between the calculated σ (averaged) and linear-theory result is approximately 0.000016, which is indicative of the degree of accuracy that can be expected with the spatial and temporal discretizations employed. In order to estimate numerical dispersion in the calculation scheme, we performed a computation at $R = 570$ with $\alpha = 0.32$ and $\epsilon = 0.00001$. The calculated wall pressure for this wave is plotted in figure 5. The non-dimensional frequency calculated from the signal is 0.1235: the corresponding linear-theory result is 0.1249. Having established that reasonably accurate results may be expected from the numerical computations when $N = 32$ and $CFL = 0.1$, we now present some results that pertain to finite-amplitude motions.

According to linear stability theory, all infinitesimal disturbances decay for $\kappa = 0$ if $R < 583.1$. The critical wavenumber in this case is $\alpha = 0.288$. The weakly nonlinear theory presented in §3 showed that bifurcation is always supercritical near the lower branch of the neutral curve and is subcritical on the upper branch, so the flow will be unstable in a finite-amplitude sense for wavenumbers corresponding to most of the upper branch of the neutral curve. We first show that the numerical computations support the result that subcritical bifurcations cannot take place at wavenumbers that correspond to the lower branch of the neutral curve. We do this by performing a calculation at $R = 570$ with $\alpha = 0.28$, $\epsilon = 0.12$ and $K = 8$. The results are presented in figures 6 (*a–c*). In figure 6 (*a*) the disturbance energy is plotted and is found to decay as a function of time. Figure 6 (*b*) contains a plot of the rate of change of disturbance amplitude (σ) which shows that, after an initial period of positive growth, σ settles down at a negative value of about -0.00059 (the linear value is -0.00016). Amplitudes of the fundamental mode and first harmonic, plotted in figure 6 (*c*), also decay. Similar calculations were performed at $R = 570$ with $\alpha = 0.25648$ and $\epsilon = 0.05$, 0.12, 0.2. The results are consistent with the weakly-nonlinear-theory

R	α	σ_{linear}	$\sigma_{\text{calculated}}$	|Error|
570	0.25648	−0.0004523	−0.0004365	0.0000158
610	0.25648	0.0	0.0000160	0.0000160
655	0.25648	0.0004423	0.0004589	0.0000166

TABLE 1. Comparison of calculated growth rate with linear theory ($K = 4$, $t = 306$, $\epsilon = 0.0001$)

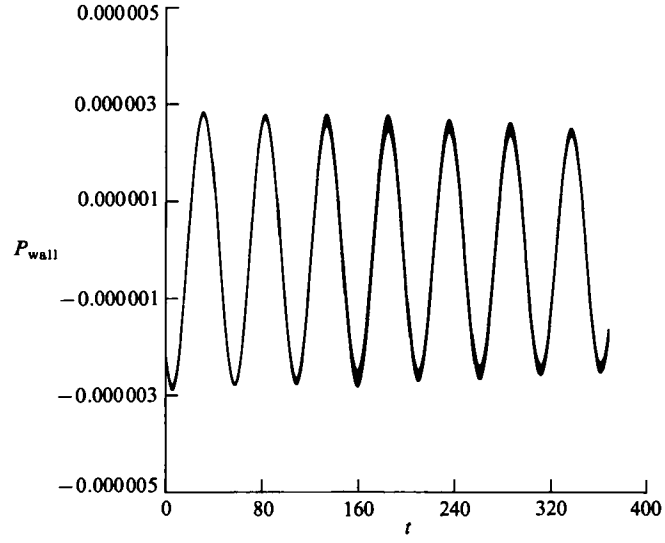

FIGURE 5. A plot of the calculated wall pressure for $R = 570$, $\alpha = 0.32$, $\epsilon = 0.00001$. Here ϵ is the initial perturbation amplitude.

result that unstable (subcritical) finite-amplitude disturbance cannot exist in a swept attachment-line boundary layer at wavenumbers that correspond to the lower branch of the neutral curve. Our full nonlinear computations do support the prediction of the weakly nonlinear theory, that subcritical instability can occur at wavenumbers that correspond to the upper branch of the neutral curve. Our computations at $R = 570$ with $\epsilon = 0.12$ and $\alpha = 0.32$, 0.33, 0.34 and 0.37 all show the existence of unstable finite-amplitude motions. The band of unstable wavenumbers at $R = 570$ lies in the range $0.28 < \alpha < 0.4$ with $\alpha = 0.34$ as the most unstable wavenumber. The results for this wavenumber are presented in figures 7 (*a–d*). Figure 7 (*a*) shows that flow energy increases with time. The disturbance growth rate is plotted in figure 7 (*b*). The magnitude of the growth rate at the time when computations were terminated was about 0.00036: the corresponding linear-theory result is −0.00099. The amplitudes of the fundamental mode and first harmonic are plotted in figure 7 (*c*), while the wall-pressure distribution is given in figure 7 (*d*). These results were obtained using $K = 8$; however, some of the computations at other wavenumbers were done using $K = 16$, and very little effect on the growth rate was found. These computations clearly show the existence of subcritical instability in the attachment-line boundary layer. In figure 8 the effect of varying Reynolds number is studied for $\epsilon = 0.12$, $\alpha = 0.34$ and $K = 8$, where the disturbance energy $E(t)$ is plotted for $R = 570$, 550, 540, and 530. It appears that for $\alpha = 0.34$ and $\epsilon = 0.12$, subcritical instability is present only for Reynolds numbers $R \geqslant 540$. At $R = 530$, $E(t)$ decays when $\epsilon = 0.12$.

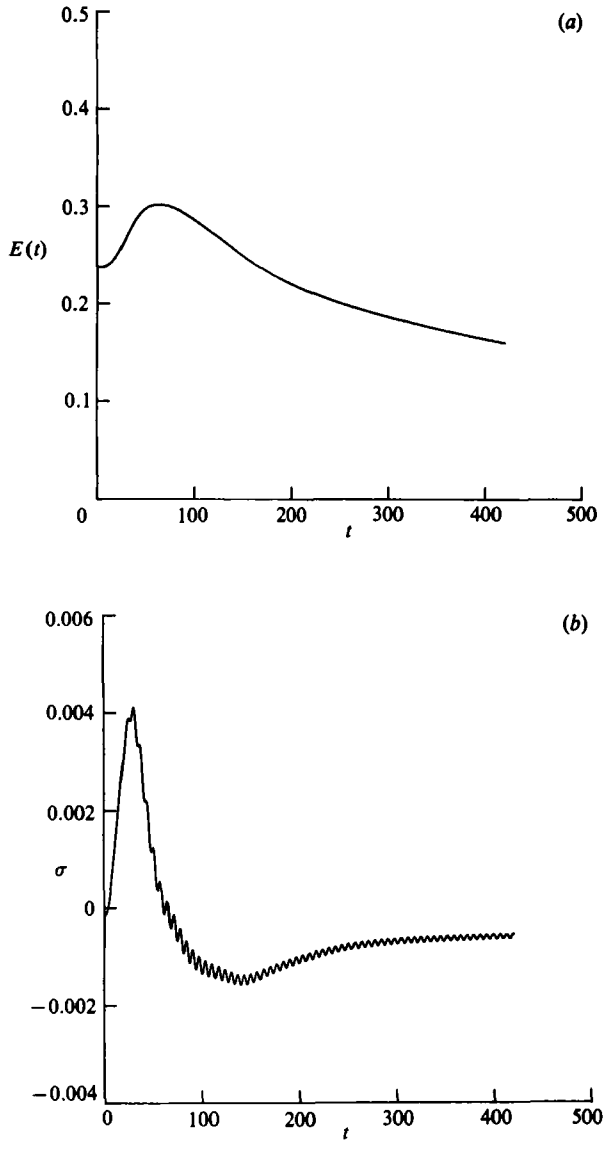

FIGURE 6(a,b). For caption see facing page.

Calculations at other wavenumbers also showed a similar trend. Higher initial disturbance amplitude may, however, trigger subcritical instability at lower Reynolds numbers. Some calculations performed at $R = 538$ showed that the growth rate increases with increasing ϵ.

A set of calculations was carried out at $R = 500$ with $\epsilon = 0.15$ and 0.2; the disturbances at all the wavenumbers decayed. In figure 9(a–c) we present the results of these calculations for $\alpha = 0.35$, $K = 16$. The growth rate at the end of the computation is about -0.00051, whilst the corresponding linear value is -0.00197. A summary of all the computations at subcritical Reynolds numbers is presented in table 2. Based on these computations it appears that subcritical instability could exist in a swept attachment-line boundary layer only at Reynolds numbers in excess of

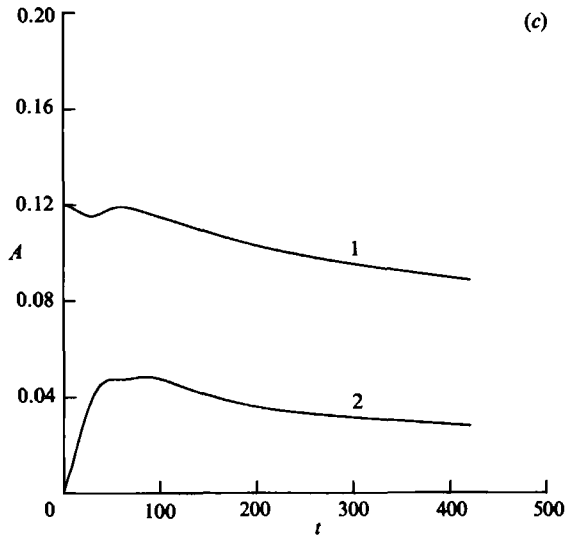

FIGURE 6. Computed results for $R = 570$, $\alpha = 0.28$, $\epsilon = 0.12$. (*a*) Disturbance energy, (*b*) Disturbance growth rate. (*c*) Amplitude of fundamental mode, 1, and the first harmonic, 2.

about 535 with reasonable amplitudes of initial disturbances. The experimental points of Pfenninger & Bacon (1969) below this Reynolds number may have been influenced by three-dimensional disturbances.

We now come to the question of the supercritical bifurcation near the lower branch of the neutral curve as predicted by the weakly nonlinear theory. For the bifurcation to be supercritical, a neutrally stable solution should exist at supercritical Reynolds numbers. We investigated this result by performing a computation at $R = 900$ and $\alpha = 0.201178$. For these conditions the linear growth rate is 0.00065. We chose an initial amplitude $\epsilon = 0.04$ and a streamwise resolution with $K = 8$. As shown in figure 10(*a*) the energy solution settles down at a constant value. This is confirmed by plotting the growth rate σ (figure 10*b*), which attains a value of approximately zero at large t for $\epsilon = 0.04$. The amplitude of the fundamental mode is plotted in figure 10(*c*). The final value is 0.0398, in excellent agreement with the weakly nonlinear prediction of 0.04. In order to see the effect of initial disturbance, two solutions were obtained with $\epsilon = 0.02$ and $\epsilon = 0.06$, and are also plotted in figure 10. It is quite clear that they too tend to the same finite-amplitude solution.

Another calculation was performed at the same wavenumber, but at a higher Reynolds number of 1000. According to the weakly nonlinear theory, the equilibrium amplitude should be about 0.056 for this Reynolds number. First, a computation was performed with $\epsilon = 0.05$. The amplitude of the fundamental mode is plotted in figure 11. At the end of the computation, the amplitude is slightly above 0.06 and still increasing. The calculation was repeated with $\epsilon = 0.065$ and the result is also plotted in figure 11. We see that this solution shows an equilibrium state at an amplitude of about 0.067. The discrepancy between this and the weakly nonlinear prediction is not totally unexpected, since at this Reynolds number the contribution from the higher-order nonlinear terms will be significant.

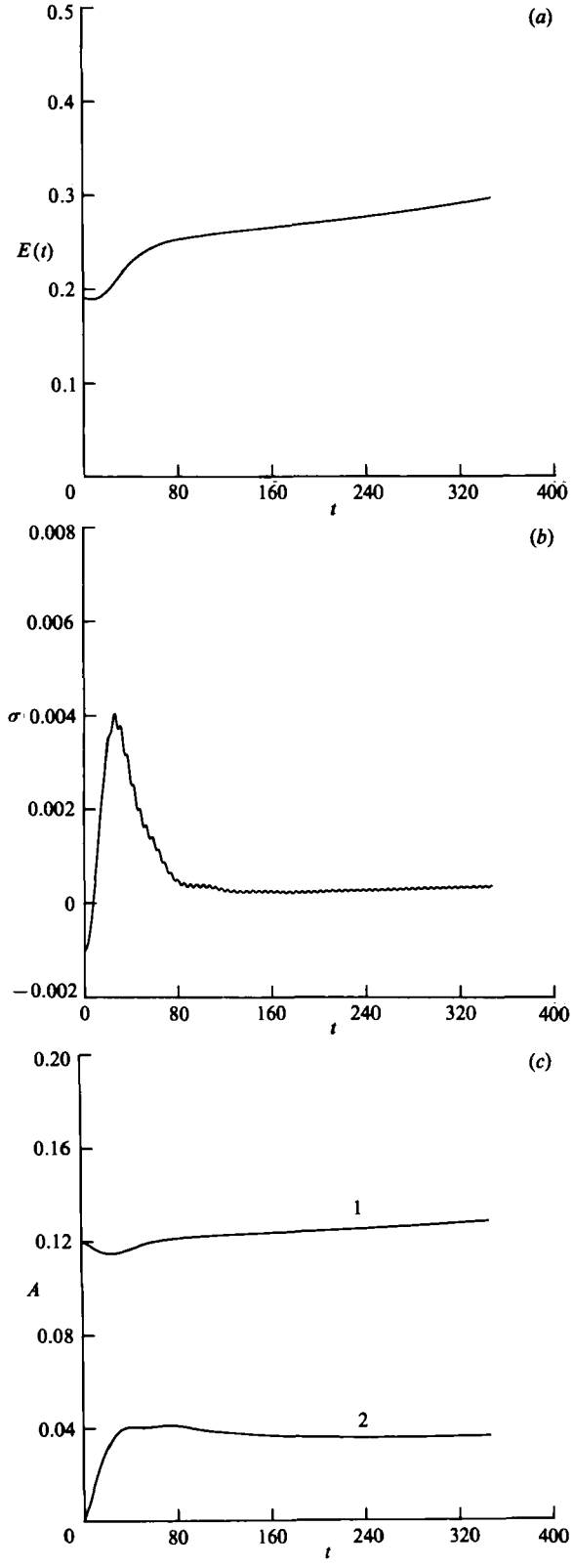

FIGURE 7 (a,b,c). For caption see facing page.

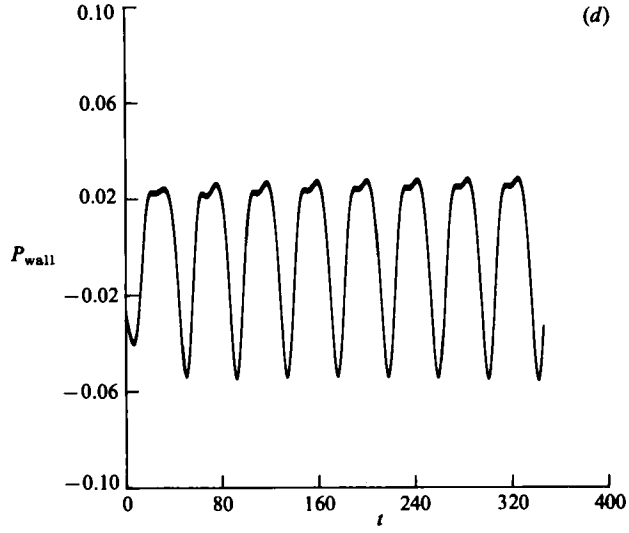

FIGURE 7. Computed results for $R = 570, \alpha = 0{,}34, \epsilon = 0.12$. (*a*) Disturbance energy. (*b*) Disturbance growth rate. (*c*) Amplitude of fundamental mode, 1, and the first harmonic, 2, (*d*) Wall pressure.

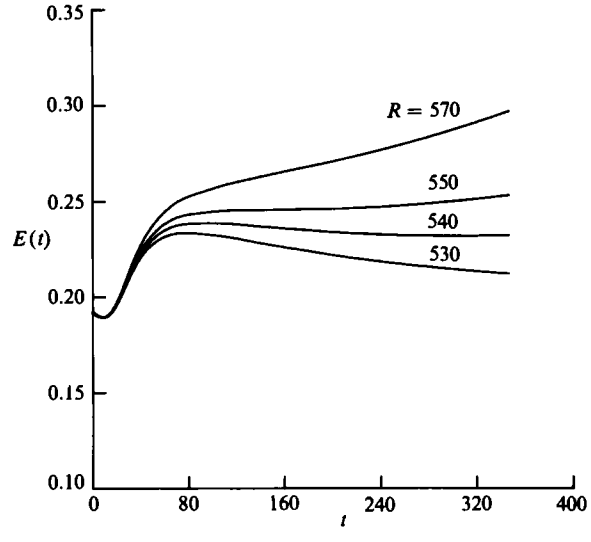

FIGURE 8. A plot of disturbance energy as a function of time for $\alpha = 0.34$ and $\epsilon = 0.12$ for four different Reynolds numbers.

5. Conclusion

The results which we have given in this paper extend the linear theory of I into both the weakly and fully nonlinear regions using asymptotic and numerical means. There seems little doubt that the absence of any upper-branch modes in the experiments of Pfenninger, Bacon, and Poll is due to the subcritical nature of the bifurcation along most of the upper branch. Furthermore, this subcritical bifurcation is the cause of the nonlinearly unstable disturbances which are investigated numerically in §4. These disturbances exist below the linear critical Reynolds number, and the

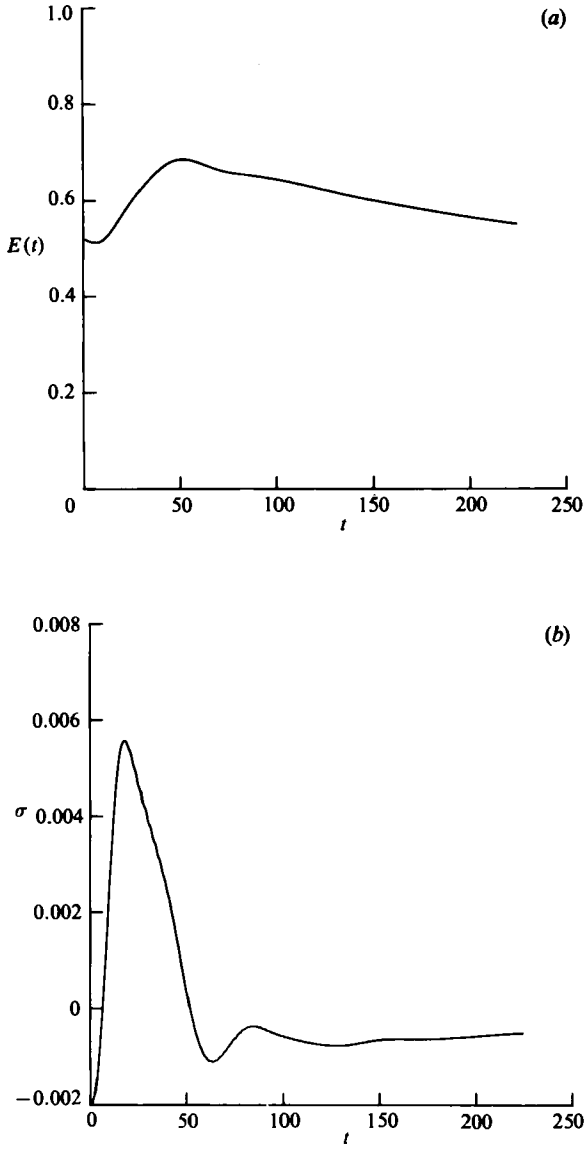

FIGURE 9 (*a*,*b*). For caption see facing page.

region in the wavenumber/Reynolds-number plane where they are unstable increases with the size of the initial amplitude. The existence of these modes is consistent with the results of Pfenninger & Bacon (1969), but, since the latter authors gave no details of the size of the disturbances introduced into the boundary layer, a quantitative comparison between experiment and theory is not possible.

Unfortunately, the expensive nature of the calculation prevented us from investigating the effect of suction or blowing on the nonlinearly unstable disturbances. It is, of course, possible to investigate particular cases if and when experimental results become available. However, it is clear from weakly nonlinear theory that the stabilizing influence of suction on transition suggested by the results of our linear calculations of I is perhaps destroyed by nonlinear effects. We refer to the fact that,

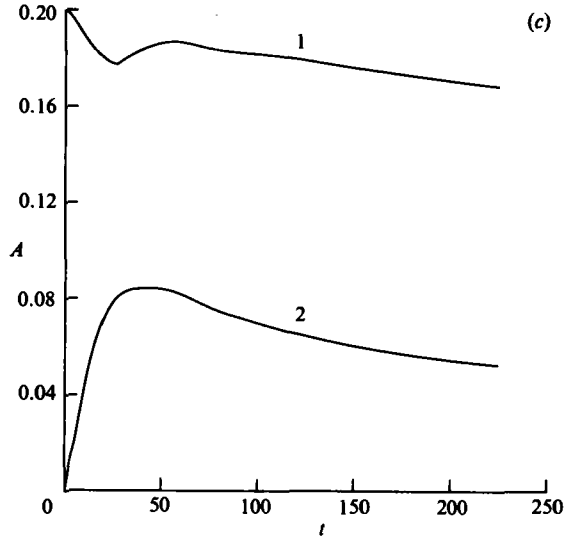

FIGURE 9. Computed results for $R = 500$, $\alpha = 0.35$, $\epsilon = 0.2$. The description is the same as in figure 6.

	R						
α	570	560	550	540	535	530	500
0.28	d	—	—	—	—	—	—
0.3	—	—	—	—	—	—	d
0.32	g	—	—	—	—	—	—
0.325	—	g	—	—	—	—	—
0.33	g	g	g	d	—	—	—
0.335	—	g	g	n	—	—	d
0.34	g	—	g	g	d	d	—
0.3425	—	—	—	g	n	d	—
0.345	—	—	—	—	—	d	—
0.35	—	—	—	—	—	d	d
0.37	g	—	—	—	—	—	d
0.4	d	—	—	—	—	—	d

TABLE 2. Summary of Navier–Stokes computations for subcritical instability (g ≡ grows, d ≡ decays, n ≡ neutral)

although the linear critical Reynolds number increases with suction, the part of the neutral curve where subcritical disturbances exist increases. Hence, if transition is in any way related to the subcritical disturbances, then the suction leads to a larger band of nonlinearly unstable modes. In contrast, if the blowing at the wall is sufficiently large, then only supercritically bifurcating modes can exist and no nonlinearly unstable modes will exist. Of course, this discussion ignores completely the role of three-dimensional disturbances in the instability-transition process, so that perhaps the most that we should assume is that the stabilizing or destabilizing effect of suction on the attachment-line instability problem is not as yet fully understood; obviously the present calculation suggests many experimental aspects of the problem which have not yet been investigated.

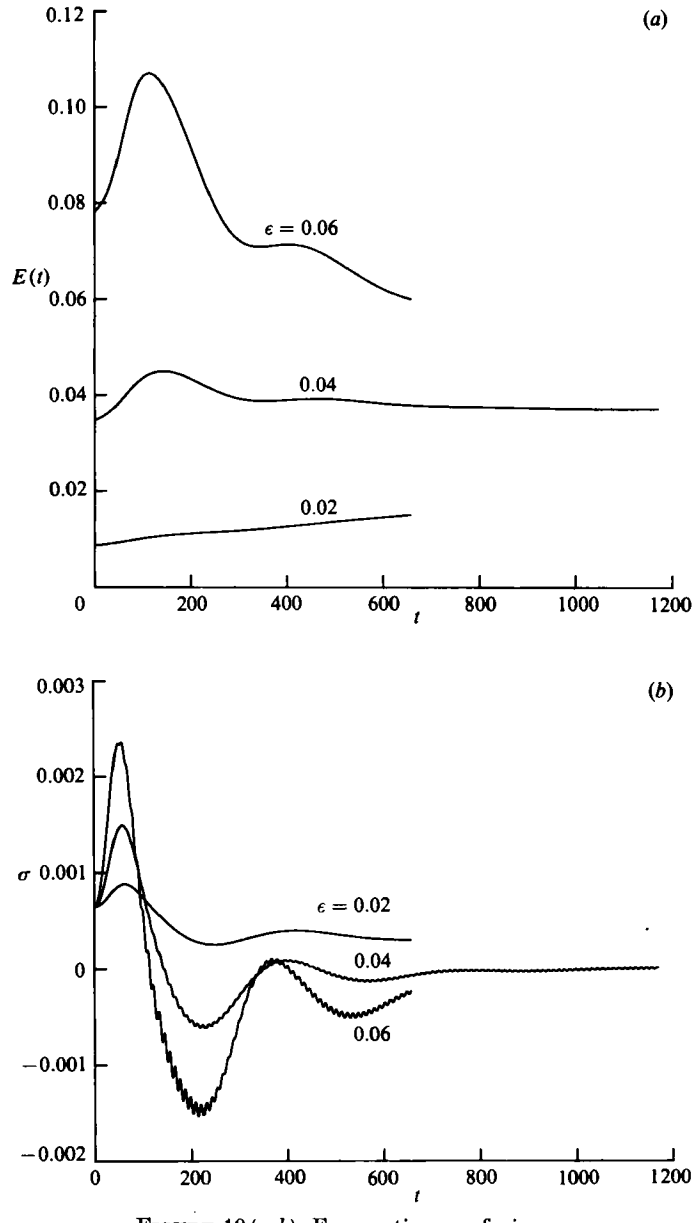

FIGURE 10(a, b). For caption see facing page.

Unfortunately, the particular X-dependence of the problem that we assumed in §2 does not generalize to oblique waves, so that this type of disturbance can only be investigated in a formally self-consistent manner using asymptotic means based on a high-Reynolds-number assumption. In any flow of practical importance the basic flow which we have considered is only the first approximation to the flow near the attachment line. It is yet to be shown how the Tollmien–Schlichting instability along the attachment line merges into a crossflow instability further away from the attachment line. There again, it seems that the only self-consistent way to investigate this problem would be to use asymptotic methods based on a high-Reynolds-number assumption.

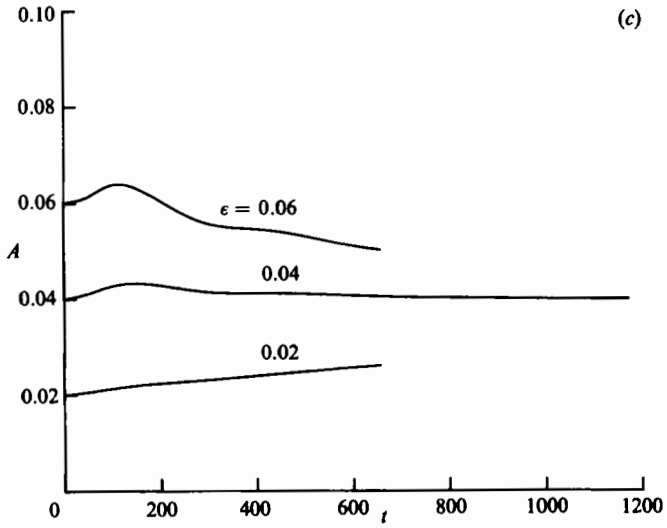

FIGURE 10. Computed results for $R = 900$, $\alpha = 0.201178$ and $\epsilon = 0.02, 0.04, 0.06$. (*a*) Disturbance energy. (*b*) Disturbance growth rate. (*c*) Amplitude of the fundamental mode.

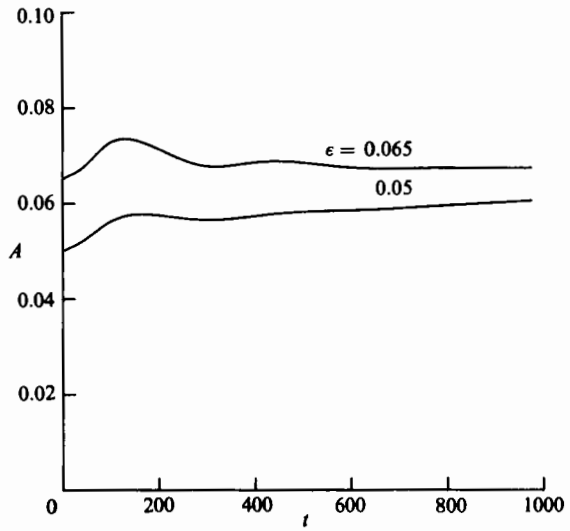

FIGURE 11. Computed amplitude of the fundamental mode for $R = 1000$, $\alpha = 0.201178$ and $\epsilon = 0.05, 0.065$.

REFERENCES

GOTTLIEB, D. & ORSZAG, S. A. 1977 *Numerical Analysis of Spectral Methods: Theory and Applications*, CBMS-NSF Regional Conference Series in Applied Mathematics, SIAM, Philadelphia.

HALL, P., MALIK, M. R. & POLL, D. I. A. 1984 *Proc. R. Soc. Lond.* A **395**, 229.

HERBERT, T. 1977 In *Laminar–Turbulent Transition, AGARD Conf. Proc.* No. 224, p. 31.

HOCKING, L. M. 1974 *Quart. J. Mech. Appl. Math.* **28**, 341.

MALIK, M. R., ZANG, T. A. & HUSSAINI, M. Y. 1984 *NASA Contractor Rep.* no. 172365, ICASE Report no. 84–19.

Moin, P. & Kim, J. 1982 *J. Fluid Mech.* **118**, 341.

Orszag, S. A. & Kells, L. C. 1980 *J. Fluid Mech.* **96**, 159.

Pfenninger, W. & Bacon, J. W. 1969 In *Viscous Drag Reduction* (ed. C. S. Wells), p. 85. Plenum Press.

Poll, D. I. A. 1979 *Aero. Quart.* **30**, 607.

Poll, D. I. A. 1980 *IUTAM Symposium on Laminar–Turbulent Transition*. Springer.

Stewartson, K. & Stuart, J. T. 1971 *J. Fluid Mech.* **48**, 529.